Available online at www.eccomasproceedia.org
Eccomas Proceedia EUROGEN (2021) 70-79

ECCOMAS
Proceedia

EUROGEN 2021
14th ECCOMAS Thematic Conference on
Evolutionary and Deterministic Methods for Design, Optimization and Control
N. Gauger, K. Giannakoglou, M. Papadrakakis, J. Periaux (eds.)
Streamed from Athens, Greece, 28–30 June 2021

CONTINUOUS ADJOINT–BASED AEROACOUSTIC SHAPE OPTIMIZATION OF AN AERO–ENGINE INTAKE

M. Monfaredi[1], V.G. Asouti[1], X.S. Trompoukis[1], K.T. Tsiakas[1] and K.C. Giannakoglou[1]

[1]National Technical University of Athens,
Parallel CFD & Optimization Unit, School of Mechanical Engineering
Zografou Campus, 9 Iroon Polytechniou Str
e-mail:morteza.monfaredi@gmail.com, vasouti@mail.ntua.gr, xeftro@gmail.com,
tsiakost@gmail.com and kgianna@mail.ntua.gr

Abstract. *This paper addresses the aeroacoustic shape optimization of a 3D aero-engine intake by means of gradient-based optimization assisted by continuous adjoint. A hybrid aeroacoustic model based on the (U)RANS equations and the permeable version of the Ffowcs Williams-Hawkings (FW-H) acoustic analogy in the frequency domain is used. The flow and adjoint simulations are for compressible fluid flows realized using the in–house GPU–enabled software PUMA. The continuous adjoint formulation includes the differentiation of the Spalart–Allmaras turbulence model. The implementation and differentiation of the 3D FW–H analogy are verified by comparing the results of the FW–H analogy to both analytical solutions and URANS. In order to save computational cost, periodic boundary conditions are used to reduce the solution domain size together with the use of a moving reference frame which leads to steady flow and adjoint runs. The generatrix of the nacelle lips and the throat area are parameterized using NURBS. The developed tool is used to perform shape optimization to minimize the total energy contained in the spectrum of the sound pressure, at prescribed receiver locations.*

Keywords: Aeroacoustic, Continuous adjoint, Shape optimization, FW-H analogy, Aero–engine Intake

Peer-review under responsibility of the organizing committee of EUROGEN 2021.
doi: 10.7712/140121.7951.18377

1 INTRODUCTION

The design of future aircraft engines and their components is a long, tedious and complicated process, involving many scientific and technical disciplines such as aerodynamics, thermodynamics, structural mechanics and acoustics, to name a few. Among them, the acoustic performance is becoming increasingly important due to ever stricter regulations related to airframe and engine emitted noise. The design trend for future civil aircraft engines is towards high and ultra high by-pass ratio engines, for which the blade tips of the large diameter fan are a very important source of noise generation. In addition, the design of the intake is of paramount importance since it is responsible for providing a uniform air supply to the engine while, at the same time, regulating the fan noise propagation towards far–field. This paper focuses on the latter.

Efficient gradient–based optimization relies upon adjoint methods, as the cost of the sensitivity computation is independent of the number of design variables [1]. Adjoint methods have been a major research topic in aerodynamic shape optimization [8, 12], recently also penetrating into the field of acoustic noise reduction [2, 3, 4, 9]. This is mainly due to the unsteady nature of the acoustic problems requiring a time–accurate adjoint solver which, increases memory requirements as the adjoint equations must be solved backwards in time. So far, mostly discrete adjoints are used in aeroacoustic shape optimization [2, 3, 4]. In one of the first works on the use of adjoint to hybrid acoustic models, [2] turbulent blunt trailing edge noise is reduced by means of the discrete adjoint to the URANS/FW–H analogy. In [9], the continuous adjoint was developed for URANS/FW–H analogy which was tested for pitching airfoils in inviscid flow. With reference to engine–intakes, the continuous adjoint to the linearized Euler equations to optimize the shape of a turbofan inlet duct, can be found in [5].

Herein, an aeroacoustic shape optimization method is developed for an aero–engine intake. This is based on the in–house GPU–enabled CFD software PUMA [6] which solves the (U)RANS equations and extends its continuous adjoint solver initially developed for aerodynamic shape optimizations. The primal and adjoint problems are solved on a cluster of GPUs, exploiting the CUDA environment as well as the MPI protocol for communications among different computational nodes. The sensitivity derivatives computation accounts for variations in turbulence quantities w.r.t. shape changes as it also solves the adjoint to the Spalart–Allmaras turbulence model.

The primal and adjoint solver of PUMA have recently been extended to computational aeroacoustics (CAA) using the FW–H analogy [9]. The hybrid (U)RANS/FW–H model and its adjoint counterpart have been implemented in PUMA based on the permeable version of the FW-H acoustic analogy in the frequency domain. This model provides the sound pressure at the receivers by computing a low–cost surface integral which depends on flow field data.

In this paper, the developed method is used to optimize the shape of an aero–engine intake, Fig. 1, by minimizing the total energy contained in the sound pressure spectrum at a set of receivers. A NURBS model is used to parameterize the shape of the nacelle lips and the throat area of the engine.

2 HYBRID ACOUSTIC MODEL

2.1 CFD Analysis Tool

The in–house GPU–enabled software PUMA is used to numerically solve the 3D (Unsteady) Reynolds-Averaged Navier-Stokes ((U)RANS) equations, [6]. This is based on a vertex-centered finite volume technique for the spatial discretization on unstructured grids and the

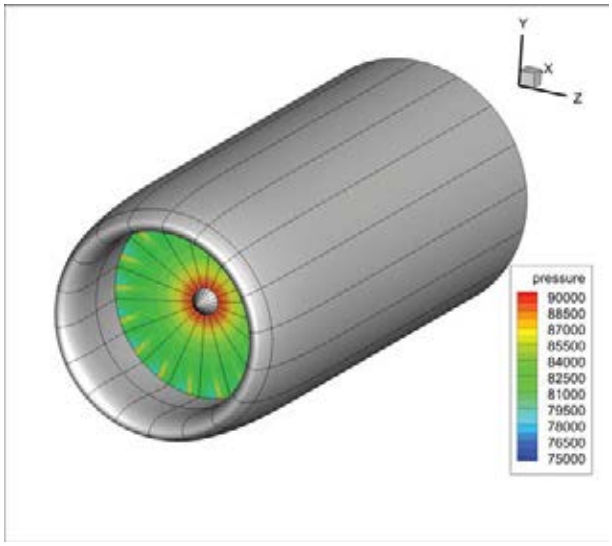

Figure 1: Perspective view of the engine intake with a snapshot of isobar contours at the engine inlet, serving as instantaneous boundary condition.

upwind second–order Roe approximation for the convection terms. The Spalart–Allmaras turbulence model [7] is used. The software implements mixed–precision arithmetics according to which the Jacobian of the residuals is computed in double– but stored in single–precision which speeds up the computations and reduces the required GPU memory, without damaging accuracy.

2.2 Noise Propagation Using The FW–H Analogy

Acoustic analogies propagate the flow–generated sound by means of analytical solutions of the wave equation and this leads to a considerable reduction in computational cost [10]. The mathematical formulation of the permeable version of the FW-–H analogy, used herein, originates from [11] for cases with a uniform mean flow (as in a wind tunnel), and reads

$$\left(\frac{\partial^2}{\partial t^2}+u_{\infty i}u_{\infty j}\frac{\partial^2}{\partial x_i \partial x_j}+2u_{\infty i}\frac{\partial^2}{\partial x_i \partial t}-c_\infty^2\frac{\partial^2}{\partial x_i \partial x_i}\right)(H(f)\rho')=\frac{\partial}{\partial t}(\mathcal{Q}\delta(f))-\frac{\partial}{\partial x_i}(\mathcal{F}_i\delta(f)) \quad (1)$$

where $H(f)$ and $\delta(f)$ are the Heaviside and Dirac delta functions, respectively. Values f=0 indicate the user–defined FW–H surface which should include all acoustic sources. Practically, f is the signed distance from this surface, with negative and positive values corresponding to its interior and exterior, respectively. The FW–H surface is located in the part of the grid which is not displaced during the optimization. c_∞ and $\vec{u}_\infty$ are the sound speed and velocity at far–field. The quadrupole effects have not been included due to their small effect and the disproportionate high computational cost. Only monopole ($\mathcal{Q}$) and dipole ($\mathcal{F}_i$) source terms

$$\begin{aligned}\mathcal{Q}(\vec{x},t) &= \left(\rho u_i - \rho_\infty u_{\infty i}\right) n_i^{\text{FWH}} \\ \mathcal{F}_i(\vec{x},t) &= \left[\rho\left(u_i - 2u_{\infty i}\right)u_j + \rho_\infty u_{\infty i}u_{\infty j} + p\delta_{ij} - \tau_{ij}\right] n_j^{\text{FWH}}\end{aligned} \quad (2)$$

are retained. $\rho = \rho_\infty + \rho'$, $p = p_\infty + p'$ and $u_i = u_{\infty i} + u_i'$ are the density, pressure and velocity components, respectively, and the subscript ∞ indicates far–field quantities. $\vec{n}^{\text{FWH}}$ is the outward unit vector normal to the FW–H surface.

The integral solution to eq. 1 provides the acoustic pressure at a receiver located at $\vec{x}_r$. For each frequency (ω) value, this yields

$$H(f)\hat{p}'(\vec{x}_r,\omega) = -\int_{f=0} \hat{\mathcal{F}}_i(\vec{x}_s,\omega)\frac{\partial \hat{G}(\vec{x}_r,\vec{x}_s,\omega)}{\partial x_{s_i}}ds - \int_{f=0} \mathrm{i}\omega\hat{\mathcal{Q}}(\vec{x}_s,\omega)\hat{G}(\vec{x}_r,\vec{x}_s,\omega)ds \tag{3}$$

where the hat $\hat{}$ symbol indicates quantities after transformation into the frequency domain using Fourier transform, i is the unit complex number and $\vec{x}_s$ denotes position vectors of sources located on the FW–H surface. In subsonic flows, the Green function for 3D problems in the frequency domain is

$$\hat{G}(\vec{x}_r,\vec{x}_s,\omega) = -\frac{\exp(-\mathrm{i}kr^+)}{4\pi r^*} \tag{4}$$

where $k = \omega/c_\infty$ is the wave number and

$$r^+ = \frac{1}{\beta^2}\Big(r^* - \frac{\vec{u}_\infty\cdot\vec{r}}{c_\infty}\Big), \quad r^* = \sqrt{\Big(\frac{\vec{u}_\infty\cdot\vec{r}}{c_\infty}\Big)^2 + |\vec{r}|^2\,\beta^2}, \quad \vec{r} = \vec{x}_r - \vec{x}_s \tag{5}$$

Also, $\beta = \sqrt{1-M^2}$ where M is the Mach number.

3 CONTINUOUS ADJOINT TO THE HYBRID ACOUSTIC MODEL

The aeroacoustic objective function J is defined in the frequency domain as the energy contained in the sound spectrum

$$J = \frac{1}{N_r}\sum_{a=1}^{N_r}\int_{\omega} |\hat{p}'(\vec{x}_{r_a},\omega)|\mathrm{d}\omega \tag{6}$$

where $\hat{p}'(\vec{x}_{r_a},\omega)$ is the outcome of eq. 3 and N_r is the number of receivers. $|\hat{p}'| = \sqrt{\hat{p}'^2_{Re} + \hat{p}'^2_{Im}}$, where subscripts Re and Im denote the real and imaginary parts of complex variables. For the purpose of this study, integration in eq. 6 degenerates to a single frequency value, namely that of the main (tonal) frequency.

To formulate the adjoint problem, an augmented objective function is defined as $J_{aug} = J + \int_{T_s}\int_{\Omega} \Psi_n R_n d\Omega dt$, where Ψ_n, R_n and Ω are the adjoint variable fields, the residuals of the unsteady flow including Spalart–Allmaras turbulence model equations and the CFD domain, respectively. T_s is the time window of the unsteady solution. By differentiating J_{aug} w.r.t. design variable b_e ($e=1,N$ with N being the number of design variables) and setting the multipliers of the derivatives of the flow variables w.r.t. b_e equal to zero within the field and along the boundaries, the unsteady adjoint equations and their boundary conditions are obtained as (only for the mean–flow equation; for the adjoint to the Spalart–Allmaras model, the reader should refer to [13])

$$-\frac{\partial\Psi_m}{\partial t} - \frac{\partial f^{inv}_{nk}}{\partial U_m}\frac{\partial\Psi_n}{\partial x_k} - \Big(\frac{\partial\tau^{adj}_{qk}}{\partial x_k} - \frac{\partial\Psi_5}{\partial x_k}\tau_{kq}\Big)\frac{\partial u_q}{\partial U_m} - \frac{\partial q^{adj}_k}{\partial x_k}\frac{\partial T}{\partial U_m} - \frac{\partial J}{\partial U_m}\delta(f) = 0 \tag{7}$$

where U_m, T and f^{inv}_{nk} are the conservative flow variables, temperature and inviscid fluxes, respectively, and

$$\tau^{adj}_{mk} = (\mu+\mu_t)\left[\frac{\partial\Psi_{m+1}}{\partial x_k} + \frac{\partial\Psi_{k+1}}{\partial x_m} + \frac{\partial\Psi_5}{\partial x_m}u_k + \frac{\partial\Psi_5}{\partial x_k}u_m - \frac{2}{3}\delta_{mk}\left(\frac{\partial\Psi_{l+1}}{\partial x_l} + \frac{\partial\Psi_5}{\partial x_l}u_l\right)\right]$$

$$q^{adj}_k = \mathcal{C}_p\left(\frac{\mu}{\mathrm{Pr}} + \frac{\mu_t}{\mathrm{Pr_t}}\right)\frac{\partial\Psi_5}{\partial x_k}$$

The last term in eq. 7 is defined only along the permeable FW–H surface. For the differentiation of this term one should refer to [9]. The adjoint boundary condition along the solid walls is $\Psi_{m+1} n_m = 0$, where $\vec{n}$ is the unit normal to the wall. Also, $q_k^{adj} n_k = 0$ is imposed along the adiabatic walls. The sensitivities of J w.r.t. design variables can be computed as

$$\begin{aligned}\frac{\delta J}{\delta b_e} = &- \int_{T_s}\int_{\Omega} \Big[\Psi_n \Big(\frac{\partial f_{nk}^{inv}}{\partial x_i} - \frac{\partial f_{nk}^{vis}}{\partial x_i}\Big) + \tau_{mk}^{adj} \frac{\partial u_m}{\partial x_i} + q_k^{adj} \frac{\partial T}{\partial x_i}\Big] \frac{\partial}{\partial x_k}\Big(\frac{\delta x_i}{\delta b_e}\Big) d\Omega dt \\ &+ \int_{T_s}\int_{S} (p\Psi_{k+1} - \Psi_n f_{nk}^{inv} + \Psi_5 q_k + \Psi_5 u_m \tau_{mk}) \frac{\delta n_k}{\delta b_e} dS dt\end{aligned} \tag{8}$$

where f_{nk}^{vis} and τ_{mk} are the viscous fluxes and stresses.

3.1 Verification of the FW-H Analogy Implementation

In the past, the implementation of the FW-H analogy in PUMA has been verified for 2D cases [9]. In this section, the implementation is verified in a 3D problem. To do so, results of the FW-H integral, eq. 3, are compared with the analytical solution of the sound field generated by a monopole source in a uniform flow. Additionally, in order to verify the part of the code that differentiates the FW–H integral, derivatives of the objective function, eq. 6, w.r.t. the coordinates of the monopole source, $\vec{x}_s$, are computed by the code and compared with the outcome of a central second–order finite difference (FD) based on the analytical solution. The monopole source is located at the origin of the coordinate system and is exposed to a uniform flow u_∞ along the $+x$ direction, shown in 2a. The complex velocity potential of the case is

$$\phi(\vec{x}_r, \vec{x}_s, \omega) = A \exp(\mathrm{i}\omega t) \frac{\exp(-\mathrm{i}kr^+)}{4\pi r^*} \tag{9}$$

where r^+ and r^* are the same as in eq. 5 . The perturbation fields of flow variables are obtained from the real parts of $p' = -\rho_\infty(\frac{\partial \phi}{\partial t} + u_{\infty 1}\frac{\partial \phi}{\partial x})$, $u' = \nabla\phi$ and $\rho' = p'/{c_\infty}^2$. In this case, $M_\infty = 0.5$, $A = 0.004\ m^2/s$ and $\omega = 3.095\ rad/s$. The FW-H surface is a cube extending from $-0.5m$ to $0.5m$ in all three directions (see Fig. 2a), and is discretized by regular surface grids on the six faces with 400 nodes on each face. The time history of p' at a receiver located at $\vec{x}_r = (10m, 0m, 10m)$ as computed using the FW–H analogy shown in Fig. 2b perfectly matches the analytical solution. Slight, practically not visible, differences in the plotted values are due to the numerical integration on the FW-H surface. The derivatives w.r.t. to the source coordinates are also compared in Fig. 2c. The agreement between finite differences of the analytical solution and the differentiation of the FW-H is very good. As expected, the derivative w.r.t. x_{s_2} is zero.

3.2 Optimization Framework For the Rotating Frame

Adjoint–based optimization in unsteady flows may become very demanding in terms of time and memory. This is the main reason why the use of adjoint methods is comparatively restricted in aeroacoustic shape optimization. In this particular application, in order to reduce the cost and since the intake geometry is axisymmetric, a CFD domain that corresponds to a single blade passage of the fan is used, with appropriate periodicity conditions. The flow and adjoint equations are solved in a rotating (with the rotational speed of the engine) frame, thus leading to a steady-state solution for both the flow and adjoint problems. A continuous circumferential distribution of receivers at given radius and axial position is used for the computation of the objective function of eq. 6. The workflow of the aeroacoustic optimization is shown in Fig. 3.

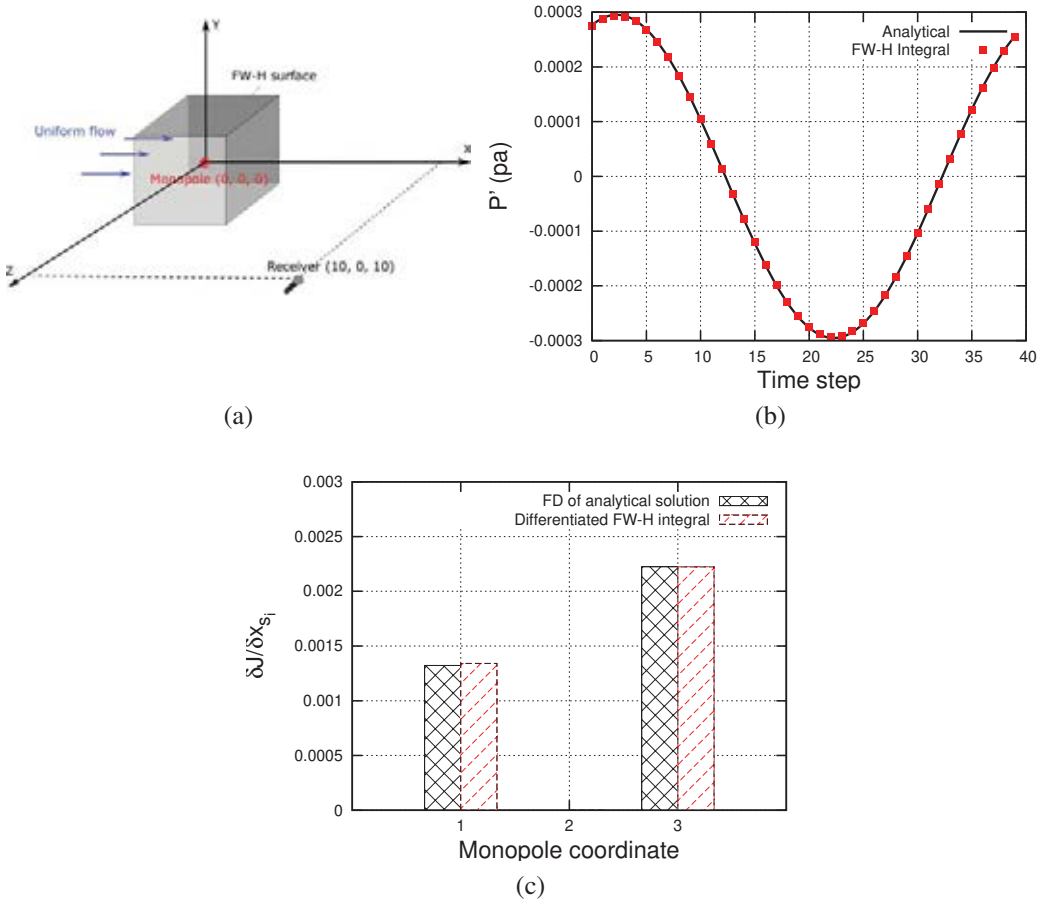

Figure 2: Results of monopole sound source in flow for a receiver located at (10m, 0m, 10m). (a) Schematic illustration of the monopole source, the FW-H surface and the receiver. (b) Comparison of the time history of pressure fluctuation within a period. (c) Comparison of the derivatives of the acoustic objective function w.r.t. to the three coordinates ($x_{s_i}, i=1,2,3$) of the monopole computed by the differentiation of the FW-H and FDs applied to the closed–form expressions.

4 SHAPE OPTIMIZATION OF THE AERO–ENGINE INTAKE

The above–described aeroacoustic analysis and optimization framework is applied to optimize an air–engine intake. The aeroacoustic objective function to be minimized, i.e. that of eq. 6, includes only the tonal noise. The geometry of a single blade passage shown in Fig. 4a has about $3.7M$ nodes arranged on 100 meridional planes. The far–field flow is still and the pressure distribution on the fan–inlet is used as boundary condition. The pressure contours on the nacelle and mid–plane of the engine intake are plotted in Fig. 4b.

An axisymmetric parameterization model is adopted for the intake. The generatrix is firstly reconstructed using NURBS and this gave rise to 15 design parameters controlling the shape of the nacelle lips and the throat area, leaving its outer shape and the part close to the fan intact. NURBS control points (CPs) are allowed to vary in both the axial and radial direction. Since the first and last points are fixed, the optimization has $2\times13=26$ design variables, Fig. 5.

The FW–H surface, illustrated in Fig. 6a, has 16000 nodes. To perform the integration of eq. 3, the FW–H surface should rotate to cover the full circumference. However, as a cheaper

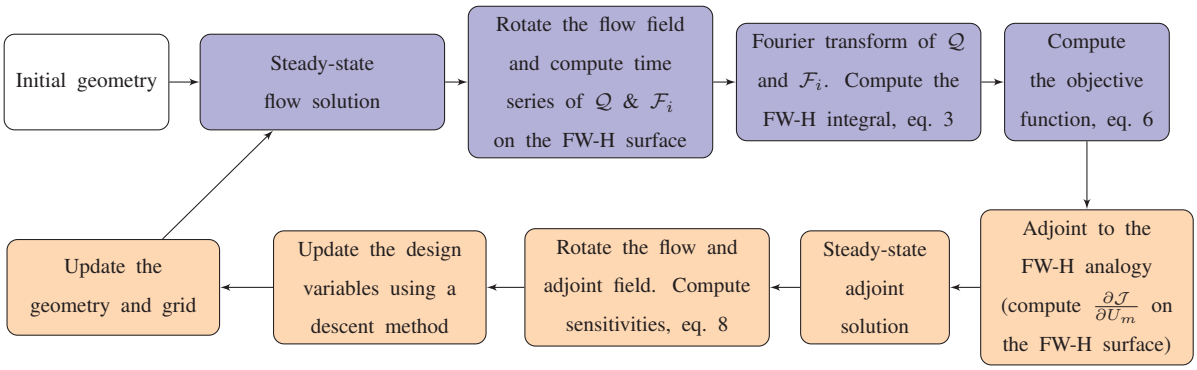

Figure 3: Workflow of the aeroacoustic optimization. Primal and adjoint parts are colored in blue and orange, respectively.

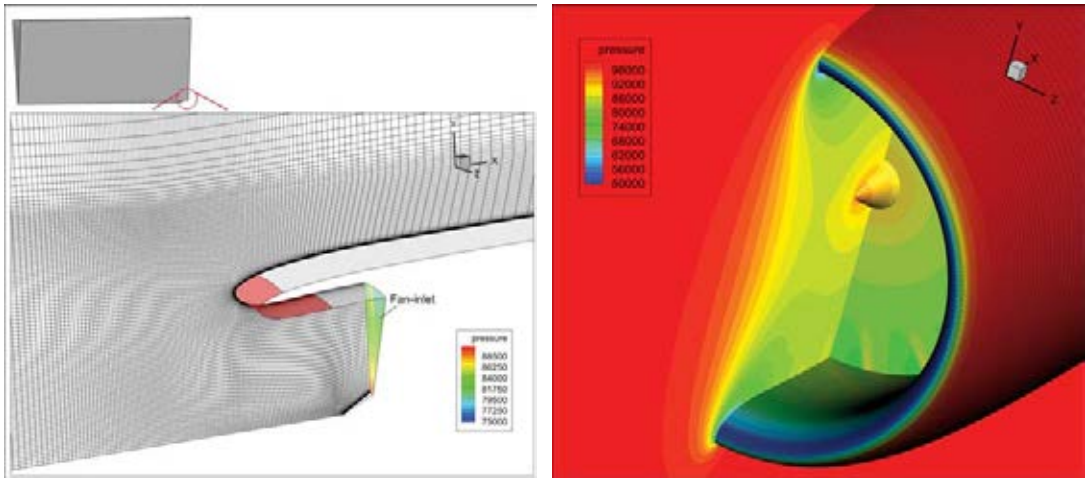

(a) (b)

Figure 4: (a) Entire and close–up views of the CFD domain and the surface grid on one of periodic boundaries. The parameterized part of the nacelle is colored in red. (b) Isobar contours on the nacelle, mid–plane and engine inlet.

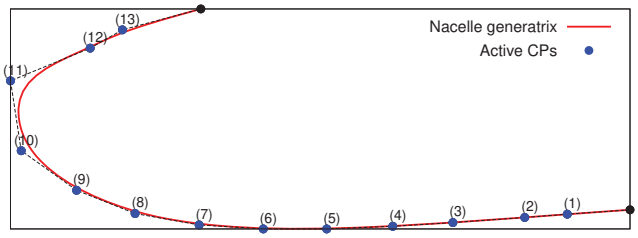

Figure 5: Distribution of the control points for the parameterization of the nacelle generatrix using NURBS. The first and last control points are fixed during the optimization.

alternative, the receivers (instead of the FW–H surface) are rotated and the acoustic pressure is retrieved by superimposing pressure signals from each receiver. As both the grid and numerical set–up may affect the acoustic results, the outcome of the FW–H analogy is verified in the current case as well. To do so, the acoustic pressure computed based on the hybrid model is

compared with that of the unsteady CFD code at 3 receiver locations, shown in Fig. 6a. The CFD results match reasonably well those obtained by the FW–H analogy, Fig. 6b, given that part of the discrepancies may be due to the neglect of quadrupole terms, representing the noise due to viscous effects and turbulence.

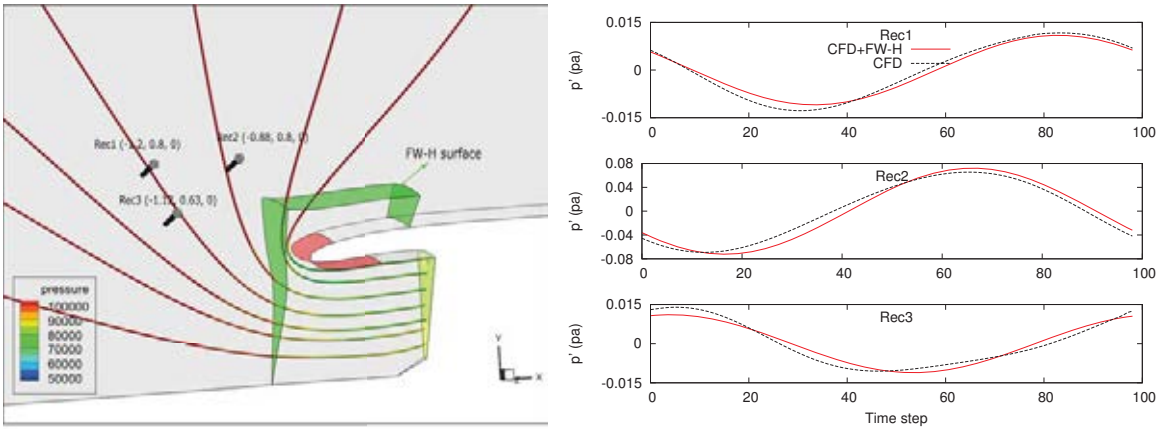

(a) (b)

Figure 6: (a) Location of the FW–H surface, in green, and 3 receivers within the CFD domain. Streamlines are colored based on the pressure values. (b) Comparison of the pressure fluctuations computed by CFD+FW–H with those obtained by pure CFD, at 3 different receivers.

The convergence history of the aeroacoustic objective function is presented in Fig. 7a. A clear reduction in the objective value after 13 optimization cycles can be seen. This reduction is also obvious in Fig. 7b that compares the amplitude of the sound pressure at a single receiver in the baseline and the optimized geometries. Changes of the parameterized part of the nacelle are illustrated in Fig. 8. As seen, the biggest geometrical change occurs at the nacelle lip which is pushed forward, while minor changes occur elsewhere. Regarding the aerodynamic performance, the optimized shape increases the total pressure loss by 0.6% compared to the initial one. This could be expected as an acoustic objective was only considered.

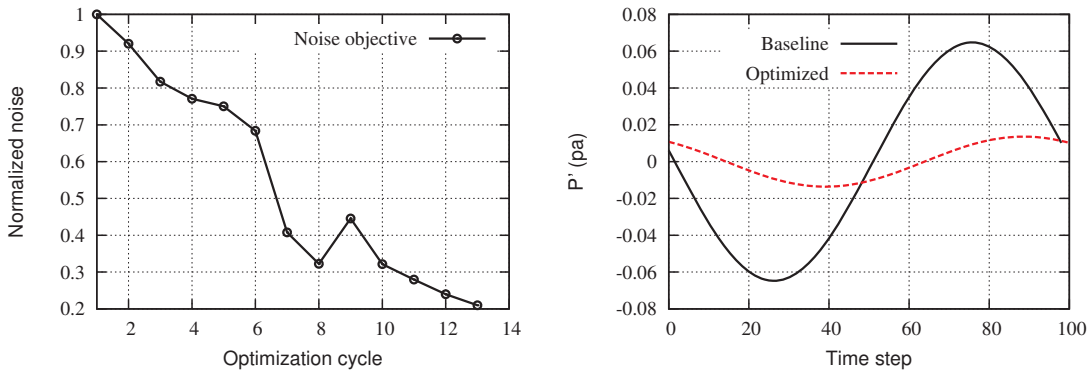

(a) (b)

Figure 7: (a) Convergence of the aeroacoustic objective value, normalized by its first cycle value. (b) Comparison of the time history of the pressure fluctuation within a period at one receiver.

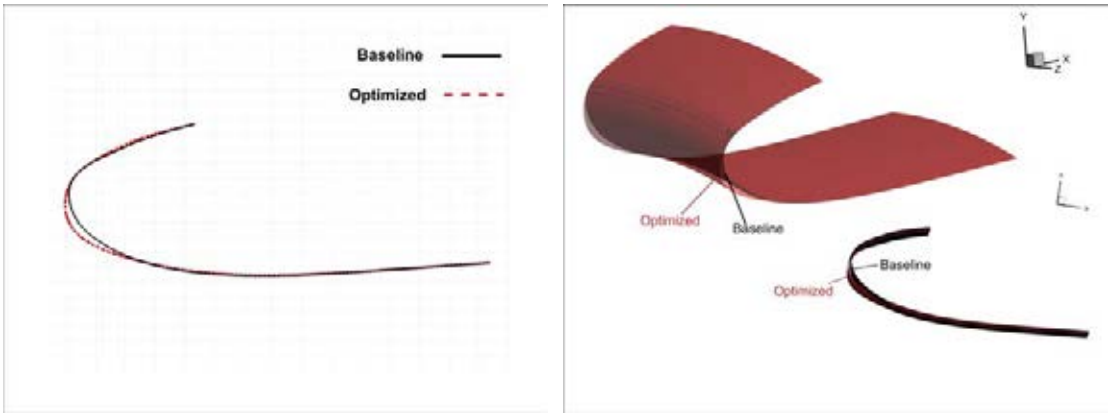

(a) (b)

Figure 8: (a) Generatrix and (b) 3D view of the baseline and optimized geometry of the parameterized part of the nacelle.

5 CONCLUSIONS

This paper presented recent extensions of the analysis and adjoint–based optimization tool of the in–house CFD solver PUMA in aeroacoustic shape optimization. A previous implementation of the permeable version of the FW–H analogy in the frequency domain, for 2D problems, is extended and verified in 3D, by comparing the results with the analytical solution of a monopole source, including its differentiation. Based on this, a feasible 3D aeroacoustic noise prediction and continuous adjoint–based shape optimization framework is developed for aero–engine intake application which makes use of a steady flow and adjoint solution and builds the unsteady field by rotating steady fields, overcoming the downsides of unsteady adjoint, namely large memory requirement and long solution time.

The developed tool is used to optimize the shape of the nacelle lips and the throat area of an aero–engine intake. The value of the aeroacoustic objective function is noticeably reduced highlighting the functionality of the developed tool. Extensions to consider both aeroacoustic and aerodynamic objectives in a multi-disciplinary framework are straightforward.

6 ACKNOWLEDGEMENTS

This work is part of the MADELEINE project which has received funding from the European Union's Horizon 2020 research and innovation programme under grant agreement No 769025. The authors would like to thank Rolls-Royce plc. (Dr. S. Shahpar) and the research group of the Institute of Sound and Vibration Research of the University of Southampton (Dr. L. Wu) for providing the initial intake geometry and the boundary conditions of the fan inlet used herein.

REFERENCES

[1] A. Jameson, Aerodynamic design via control theory. *Journal of Scientific Computing*, **3**, 233–260, 1988.

[2] M. Rumpfkeil, D.Zingg, A hybrid algorithm for far-field noise minimization. *Computers & Fluids*, **39**, 1516–1528, 2010.

[3] B.Y. Zhou, T. Albring, N.R. Gauger, C.R. Ilario da Silva, T.D. Economon, J.J. Alonso, A discrete adjoint approach for jet-flap interaction noise reduction. *58th AIAA/ASCE/AHS/ASC Structures, Structural Dynamics, and Materials Conference*, Grapevine, Texas, USA, January 9-13, 2017.

[4] R.Ö. Içke, O. Baysal, L.V. Lopes, B.Y. Zhou, B. Diskin, A. Moy, Toward adjoint-based aeroacoustic optimization for propeller and rotorcraft applications. *AIAA Aviation 2020 Forum*, Virtual, June 15-19, 2020.

[5] S. Qiu, A continuous adjoint-based aeroacoustic shape optimization for multi-mode duct acoustics. *Proceedings of the Institution of Mechanical Engineers, Part C: Journal of Mechanical Engineering Science*, **232**, 3897–3914, 2018.

[6] V.G. Asouti, X.S. Trompoukis, I.C. Kampolis, K.C. Giannakoglou, Unsteady CFD computations using vertex-centered finite volumes for unstructured grids on graphics processing units. *International Journal for Numerical Methods in Fluids* **67**, 232–246, 2011.

[7] P. Spalart, S. Allmaras, A one–equation turbulence model for aerodynamic flows. *La Recherche Aerospatiale*, **1**, 5–21, 1994.

[8] E.M. Papoutsis-Kiachagias, K.C. Giannakoglou, Continuous adjoint methods for turbulent flows, applied to shape and topology optimization: Industrial applications. *Archives of Computational Methods in Engineering*, **23**, 255–299, 2016.

[9] M. Monfaredi, X.S. Trompoukis, K.T. Tsiakas, K.C. Giannakoglou, An unsteady aerodynamic/aeroacoustic optimization framework using continuous adjoint. *Advances in Evolutionary and Deterministic Methods for Design, Optimization and Control in Engineering and Sciences. Computational Methods in Applied Sciences*, vol 55, 2021.

[10] J. Ffowcs Williams, D. Hawkings, Sound generation by turbulence and surfaces in arbitrary motion. *Philosophical Transactions of the Royal Society of London. Series A, Mathematical and Physical Sciences*, **264**, 321–342, 1969.

[11] D. Lockard, An efficient, two-dimensional implementation of the Ffowcs Williams and Hawkings equation. *Journal of Sound and Vibration*, **229**, 897–911, 2000.

[12] D.I. Papadimitriou, K.C. Giannakoglou, A continuous adjoint method with objective function derivatives based on boundary integrals for inviscid and viscous flows. *Computers & Fluids*, **36**, 325–341, 2007.

[13] K.T. Tsiakas, Development of shape parameterization techniques, a Flow solver and its adjoint, for optimization on GPUs. Turbomachinery and external aerodynamics applications. *PhD Thesis, NTUA*, 2019.